Thermochimica Acta 724 (2023) 179513

Contents lists available at ScienceDirect

Thermochimica Acta

journal homepage: www.elsevier.com/locate/tca

Kinetic analysis and modeling of paper-laminated phenolic printed circuit board (PLP-PCB) pyrolysis using distributed activation energy models (DAEMs)

Ali Shokri, Farzam Fotovat *

Department of Chemical and Petroleum Engineering, Sharif University of Technology, Tehran, Iran

ARTICLE INFO

Keywords:
Paper-laminated phenolic printed circuit board
Pyrolysis
Kinetic modeling
Thermogravimetric analysis (TGA)
Distributed activation energy model (DAEM)

ABSTRACT

This work explores the pyrolysis characteristics and kinetic behavior of paper-laminated phenolic printed circuit boards (PLP-PCBs) using thermogravimetric analysis under non-isothermal linear heating programs. The initial estimation of the kinetic parameters during the pyrolysis was obtained from the analysis of the experimental data by three isoconversional kinetic models, i.e. Flynn-Wall-Ozawa (FWO) and Kissinger-Akahira-Sunose (KAS) integral methods, as well as the Friedman differential method. For all three methods, the apparent activation energy exhibited a strong dependence on the degree of the reaction conversion. To allow for the complexity of the reactions involved in the PLP-PCB pyrolysis, two distributed activation energy models (DAEMs) with a first-order reaction function were derived by assuming the discrete and multi-Gaussian distributions for the activation energies. A six pseudo-component Gaussian DAEM was able to accurately describe the PLP-PCB pyrolysis. By applying the discrete DAEM algorithm, the pyrolysis of PLP-PCB could be precisely characterized by 37 dominating reactions.

1. Introduction

Rapid and continual technological innovations have accelerated the update and advancement of electrical and electronic devices, which engenders an expeditious replacement process generating millions of tons of electronic waste (e-waste) annually. This has made e-waste a growing global issue. According to statistical data, the worldwide production of e-waste in 2021 is estimated at nearly 55.5 million metric tons (MMT) and is projected to exceed 74 MMT by 2030 with 3–5% growth per annum [1]. Printed circuit boards (PCBs) are deemed one of the core constituents of virtually all electronic products, and the resulting waste PCBs (WPCBs) constitute approx. 6% (w/w) of the entire e-waste weight while comprising 40% of the overall metal value [2], signifying the appreciable metallic fraction included in WPCBs. The PCBs are heterogeneous mixtures of the non-conductive reinforced substrate (50 wt.%), macromolecule binder (20 wt.%), and various types of metals (30 wt.%), such as high-grade base metals (Cu, Fe, Ni, Al, Sn, and Zn) and nearly all the noble metals (e.g. Au, Ag, Pt) [3]. There are multiple types of PCBs, among which the fiberglass-reinforced epoxy resin (FRE-PCB) and the paper-laminated phenol resin (PLP-PCB) are the two most customarily used in electronic products [4]. The WPCBs also encompass copious amounts of hazardous substances (such as halogenated flame retardants, PVC, etc.) and a variety of heavy metals (such as Pb, Sb, Cd, and Cr) that may gravely contaminate the environment [5]. Therefore, the recycling of WPCBs holds far-reaching prominence not only from the high-value metal resource utilization standpoint but also from the aspect of environmental protection.

In the prior decades, many countries, private factories, and informal sectors disposed of WPCBs via simple burning and acid treating to extract metals that not only was a dissipation of the valuable metal resources but also led to the emissions of acutely hazardous substances, in particular, polybrominated dibenzodioxins/furans (PBDD/Fs) [6]. Over a decade-long effort, in furtherance of catering to the sustainable circular economy and zero environmental footprints, a series of metal recycling technologies such as mechanical-physical, chemical, pyrometallurgical, hydrometallurgical, and bio-metallurgical, or an amalgamation of these techniques have been copiously studied to retrieve valuable substances from WPCBs and plenty of advances have been achieved [7]. Nevertheless, many hard-to-tackle technical defects and economic drawbacks are remaining [8–13], such as high chemical reagent consumption, the release of toxic gas and by-product fume emissions throughout the pyrometallurgical procedures, high cost of solvent

* Corresponding author.
E-mail address: fotovat@sharif.edu (F. Fotovat).

https://doi.org/10.1016/j.tca.2023.179513
Received 25 January 2023; Received in revised form 2 April 2023; Accepted 6 April 2023
Available online 7 April 2023

recovery, and the intricate post-treatment of waste effluents and sludge forming during the hydrometallurgical processes.

Alternatively, pyrolysis, a thermochemical process in the absence of oxygen, is considered a versatile and promising waste disposal technique for the effective recovery of high-value metals and organic compounds in WPCBs, with minimal environmental implications and low capital costs [14]. Throughout this process, the resin and binder thermally degrade into low-molecular products under elevated temperatures, which then can be reprocessed to produce a variety of products such as chemical feedstock or alternative energy resources [15]. Previous studies on the pyrolysis of FRE-PCBs and PLP-PCBs showed that phenol, substituted phenols, bisphenol A, and acetone are the dominant compounds in the liquid phase products, whereas CO, CO_2, CH_4, and H_2 prevail in the gas phase [4,16–21].

Several studies have been carried out on FRE-PCBs pyrolysis to explore the pyrolysis mechanism, analyze the properties of the products, optimize the operational parameters, and suppress the release of brominated contaminants [8,22–27]. Nonetheless, a limited number of studies have been dedicated to the pyrolysis of PLP-PCBs, particularly concerning the kinetics of PLP-PCB pyrolysis. Considering the greater amounts of organic substances in PLP-PCB compared to FRE-PCB, larger quantities of pyrolysis products can be recycled from PLP-PCB and exploited as a chemical feedstock. Grause et al. [28] carried out the pyrolysis of PLP-PCB utilizing a batch reactor and a thermogravimetric analyzer/ mass spectrometer (TGA/MS) and reported the generation of large quantities of organic compounds, including levoglucosan, triphenylphosphate, phenolic compounds, and bisphenols. Moreover, it is expected that the amount of hazardous brominated compounds in the oil products acquired from PLP-PCB pyrolysis to be lower compared to FRE-PCB pyrolysis, as PLP-PCB consists of non-brominated flame retardants such as triisopropyl-phenyl phosphate (TIPPP) [17,29].

Thermogravimetric analysis (TGA) is regarded as a robust thermoanalytical technique for solid-phase kinetic studies and pyrolytic behavior characterization by accurately recording the sample weight loss while changing the sample temperature [30]. It is noteworthy that investigating the temperature region of interest in a single run is one of the pros of the non-isothermal constant heating rate analyses. Two major categories of methods, i.e., model-free and model-fitting approaches, have been developed employing TGA measurements to formulate the mathematical expressions describing the solid-state thermal decomposition. Although the isoconversional model-free approaches provide accurate estimates of the kinetic parameters without requiring prior knowledge of the reaction mechanism, their applicability is restricted in the cases of overlapped devolatilizations, secondary reactions, and catalytic effects adding further complexity to the system [31]. The model-fitting methods are preferred under the complex circumstances mentioned above. Among the model-fitting approaches, the distributed activation energy model (DAEM) is considered an accurate, versatile, and effective tool for appraising the devolatilization kinetics of various complex feedstocks [32]. In DAEM, it is assumed that an infinite number of independent, parallel, irreversible reactions with a constant pre-exponential factor and various activation energy values are in progress at any given time and temperature [33]. The activation energy distribution of these reactions, which reflects variations in the bond energies of the species, can be represented by a probability density distribution function (PDF) (e.g., the Gaussian distribution) or by a discrete distribution [34,35]. Krishna et al. [36] studied the pyrolysis kinetics of the PCBs used in a television, a motherboard, and a hard disk and developed DAEMs assuming both Gaussian and Weibull distributions for the activation energies. In the discrete DAEM, by discretization, the infinite reactions are simplified into many (but finite) independent parallel irreversible reactions; each of which follows a unique pair of activation energy and pre-exponential factor [35]. Compared to the PDF-based DAEM, the discretization of infinite reactions allows for the pre-exponential factor to vary with the activation energy, preserving the nature of intricacy in the pyrolysis process.

Though the pyrolysis kinetics of FRE-PCBs has adequately received the attention of researchers, studies have rarely explored the pyrolysis kinetics of PLP-PCBs and, to the best of our knowledge, no kinetic model has yet been exclusively proposed for their pyrolysis, despite their fast-growing use in a variety of electronic devices including the home appliances. Considering the lack of a comprehensive study on the kinetics of PLP-PCB pyrolysis, in the present study, the pyrolysis characteristics and corresponding kinetics of PLP-PCB decomposition are explored by employing the non-isothermal thermogravimetric analysis (TGA). Accordingly, the apparent activation energies during the PLP-PCB pyrolysis process are first evaluated by applying the various isoconversional model-free techniques, including Friedman, Flynn-Wall-Ozawa (FWO), and Kissinger-Akahira-Sunose (KAS). Moreover, discrete DAEM and multi-Gaussian DAEM are employed to describe the pyrolytic kinetics of PLP-PCB during the thermal degradation process. The quality of fit, the prediction potential, and the important features of the studied kinetic models are then extensively deliberated to identify the best model. This research provides a deeper understanding of the pyrolysis mechanism of PLP-PCB and can serve as a helpful reference for the proper design and optimization of the green PLP-PCB thermochemical disposal processes.

2. Materials and methods

2.1. Materials

Waste PLP-PCB samples utilized for the current study were obtained from a local waste disposal facility. They were the residue remaining after the mechanical-physical processes for copper recovery. These metal-free PLP-PCBs were first washed with deionized water to eliminate any contaminants on the surface. Afterward, the samples were disk-milled with liquid nitrogen, dried for a duration of 4 h at 105 °C, then sieved to acquire particles of size <500 μm, and preserved in sealed plastic bags for further characterization.

Physicochemical characterizations of PLP-PCB were specified using several techniques. Proximate analysis of the PLP-PCB sample was performed in accordance with the related ASTM standards [37] to measure the volatile material, fixed carbon, moisture, and ash content of the waste samples. The weight content of organic C, H, N, and S was analyzed in an elemental analyzer (LECO-TruSpec® CHNS), while the oxygen content was estimated from the mass balance: O (wt.%) = 100% - C (wt.%) - H (wt.%) - N (wt.%) - S (wt.%) - Ash (wt.%). The higher heating value (HHV) was computed by a non-linear correlation proposed by Nhuchhen and Salam [38] employing the ultimate analysis results. The composition of the residual metals was determined utilizing inductively coupled plasma-optical emission spectrometry (ICP-OES, 730-ES, Varian) after digesting through a robust procedure [18]. The non-metal and mineral compositions of the PLP-PCB sample were quantified employing X-ray fluorescence spectroscopy (XRF, Philips PW-1410). To ensure the reproducibility of the results of the analysis, they were repeated one more time if necessary. The results are tabulated in Table S1 and Table 1.

As listed in Table S1, the carbon and volatile content in PLP-PCB accounted for 41.16 and 75.89 wt.%, respectively, which are much higher compared to the respective values reported for FRE-PCB in the literature [17]. However, the bromine and the ash contents of the PLP-PCB used in this study were 1.7 and 1.04 wt.%, which is substantially less than the reported average of 5.41 and 68.1 wt.% for FRE-PCB [39]. These properties of PLP-PCB connote its potential value for producing larger quantities of cleaner chemical feedstock relative to FRE-PCB.

2.2. Thermogravimetric analysis

The pyrolysis of the PLP-PCB was carried out in a simultaneous thermogravimetric analyzer (TG/DSC 1 STAR, Mettler Toledo USA)

Table 1
Chemical constituents of the investigated PLP-PCB samples.

	Cu	Al	Fe	Ni	SiO_2	Al_2O_3	CaO	NaO_2	TiO_2
wt.%	0.06	BDL	BDL	BDL	0.071	0.364	0.221	0.071	0.026

*BDL: below detection limit.

under atmospheric pressure. A non-reactive environment was maintained during pyrolysis by continuous purging with 50 mL min^{-1} of pure nitrogen gas. Approximately 10.0 ± 0.5 mg of samples were weighed, placed into an α-alumina crucible, and then heated from 25 to 800 °C at four different constant heating rates of 10, 15, 20, and 30 °C min^{-1}. Stabilization of pyrolysis prior to initiation and after completion was ensured by adding an extra isothermal step before and after the linear heating program. Each TG test was performed twice to confirm accuracy and precision, and for each run, the TG measurements were repeated for the third time only if either the data were noisy or the discrepancy detected in the conversion values was more significant than 5.0%.

2.3. Kinetic modeling

2.3.1. Theoretical background

For a single-step global reaction regime, the heterogeneous solid-state pyrolysis reaction rate during the linearly heated non-isothermal TGA process could be interpreted as a basic homogeneous kinetic coupled with the Arrhenius law for the rate constant [40]. The differential form of such a rate equation can be defined as:

$$\frac{d\alpha}{dT} = \frac{A}{\beta}\exp\left(-\frac{E_a}{RT}\right)f(\alpha) \tag{1}$$

where E_a and A are the apparent activation energy (J mol^{-1}) and apparent pre-exponential coefficient (s^{-1}), respectively; T denotes the absolute temperature (K); R represents the ideal gas constant (8.3145 J $mol^{-1}K^{-1}$); β is the linear heating rate ($\beta = dT/dt = const.$, K s^{-1}); α is the extent of conversion (Eq. (2)), and $f(\alpha)$ indicates the reaction mechanism model, describing the dependency of the rate of the reaction progression upon the extent of the reaction, α.

$$\alpha = \frac{m_0 - m(t)}{m_0 - m_\infty} \tag{2}$$

where m_0 and m_∞ are the primary and residual sample mass in the pyrolysis process, respectively, while $m(t)$ denotes the instantaneous sample mass at a given time t / temperature T. The integral form of Eq. (1), after separating α and T variables, is obtained as:

$$g(\alpha) = \int_0^\alpha \frac{1}{f(\alpha)}d\alpha = \frac{A}{\beta}\int_{T_0}^{T}\exp\left[-\frac{E}{RT}\right]dT = \frac{A}{\beta}\psi(E,T) \tag{3}$$

where $g(\alpha)$ designates the integral form of the chemical reaction model $f(\alpha)$; T_0 is the initial pyrolysis temperature (K); and $\psi(E,T)$ is the temperature-integral. Although there is no exact analytical solution for the temperature-integral term in Eq. (3), it is customarily solved by employing either numerical integration or mathematical approximations.

2.3.2. Iso-conversional method

The isoconversional kinetic models are based on two basic assumptions: (i) at any constant conversion (α_i), the reaction rate is solely a function of temperature (ii) the reaction model [$f(\alpha)$] and the kinetic parameters, i.e. E, A, at any particular conversion level are independent of the heating rate. These methods are classified as model-free approaches since they do not require preliminary information regarding the reaction mechanism model [41]. Several isoconversional kinetic models have been developed so far. Based on the form of the employed reaction mechanism model, the isoconversional methods are generally subdivided into either differential or integral approaches. The Friedman, Flynn-Wall-Ozawa (FWO), and Kissinger-Akahira-Sunose (KAS) isoconversional kinetic models were chosen in this study owing to their previously successful application in studying solid-state decomposition [42].

Though the differential isoconversional kinetic methods are prone to data noise, they are helpful to predict the kinetic parameters [43]. The Friedman isoconversional method [44], (Eq. (4)), is one of the most straightforward and commonly implemented differential solutions to Eq. (1).

$$\ln\left(\frac{d\alpha}{dt}\right)_{\alpha_i} = \ln[A_\alpha f(\alpha)] - \frac{E_\alpha}{R\cdot T_{\alpha_i}} \tag{4}$$

where $\left(\frac{d\alpha}{dt}\right)_{\alpha_i}$, $T_{\alpha i}$, E_α, and A_α denote the conversion rate, temperature, apparent activation energy, and pre-exponential factor at a particular level of conversion α_i, respectively. Linear fitting between $\ln\left(\frac{d\alpha}{dt}\right)_{\alpha_i}$ and $\left(\frac{1}{T_{\alpha_i}}\right)$ gives a line with the slope of $-\frac{E_\alpha}{R}$. The shape of derivative thermogravimetric (DTG) curves or $\left(\frac{d\alpha}{dt}\right)$ as a function of temperature renders valuable information concerning the degradation mechanism, e.g., whether the degradation process consists of a single reaction or rather multiple reactions [45].

The FWO integral solution [46] of Eq. (3) is represented by Eq. (5).

$$\ln\beta_i = \ln\left[\frac{A_\alpha E_\alpha}{R\ .\ g(\alpha)}\right] - 5.331 - 1.052\left(\frac{E_\alpha}{R\cdot T_{\alpha_i}}\right) \tag{5}$$

The slope of linearly fitted lines of the $\ln(\beta_i)$ vs. $\left(\frac{1}{T_{\alpha_i}}\right)$ graph is employed to appraise the apparent E_α.

The integral solution of Eq. (3) proposed by KAS [47] is given by:

$$\ln\left(\frac{\beta_i}{T_{\alpha_i}^2}\right) = \ln\left[\frac{A_\alpha R}{E_\alpha\ .\ g(\alpha)}\right] - \frac{E_\alpha}{R\cdot T_{\alpha_i}} \tag{6}$$

For a given conversion level α_i, the E_α is estimated from the corresponding slope of the linear fitting lines of the graph between $\ln\left(\frac{\beta_i}{T_{\alpha_i}^2}\right)$ and $\left(\frac{1}{T_{\alpha_i}}\right)$.

2.3.3. Distributed activation energy model

The distributed activation energy model (DAEM) follows the hypothesis that the entire reaction regime consists of an unlimited number of independent and irreversible decomposition reactions occurring simultaneously. All such reactions are assumed to share a constant pre-exponential factor, while the variation in activation energies is presented by a continuous probability distribution [48]. The standard form of first-order DAEM for the linearly heated non-isothermal pyrolysis process is described by Eq. (7) [49]:

$$\alpha(T) = 1 - \int_0^\infty \exp\left[-\int_{T_0}^{T}\frac{A}{\beta}\exp\left(-\frac{E}{RT}\right)dT\right]f(E)dE \tag{7}$$

where $f(E)$ denotes the continuous distribution function of activation energy, representing the discrepancies in the activation energies of presumed first-order irreversible reactions. Various forms of $f(E)$, including Gaussian, Weibull, Logistic, and Gamma distribution, were

employed in pyrolysis kinetic studies [50]. In this study, to evaluate the kinetic parameters, the Gaussian distribution (as shown in Eq. (8)) was selected and investigated on account of the success of this type of modeling in similarly complex materials [51].

$$f(E) = \frac{1}{\sigma_E\sqrt{2\pi}}\exp\left[-\frac{(E-E_0)^2}{2\sigma_E^2}\right] \tag{8}$$

where E_0 and σ_E are the mean activation energy (kJ mol^{-1}) and the corresponding standard deviation, respectively. The derivative of Eq. (7) with respect to T is given by Eq. (9):

$$\frac{d\alpha}{dT} = \int_0^{\infty}\frac{A}{\beta}\exp\left[-\frac{E}{RT} - \int_{T_0}^{T}\frac{A}{\beta}\exp\left(-\frac{E}{RT}\right)dT\right]f(E)dE \tag{9}$$

To accurately describe the multi-reaction regimes of complex materials, DAEM with the Gaussian distribution model can be further segmented into multiple fractions, each corresponding to a pseudo-component. Furthermore, it is presumed that there are no interactions amongst such pseudo-components, and the pyrolytic kinetics of each pseudo-component is expressed by a single Gaussian DAEM. Thus, the overall extent of conversion is expressed as Eq. (10).

$$\alpha(T) = \sum_{j=1}^{m} c_j\alpha_j(T) \text{ and } \frac{d\alpha}{dT} = \sum_{j=1}^{m} c_j\left(\frac{d\alpha}{dT}\right)_j, \sum_{j=1}^{m} c_j = 1 \tag{10}$$

where $\alpha_j(T)$ represents the extent of conversion for j^{th} pseudo-component, and m denotes the number of pseudo-components. In Eq. (10), c_j is referred to as the composition factor and indicates the portion of volatiles that evolved from the j^{th} pseudo-component in the mixture.

To estimate the kinetic parameters of multi-DAEM (A_i, E_{0i}, σ_{Ei}, and c_i), Eq. (11) defines an objective function (residual sum of square or *RSS*) formulated on conversion rate $\left(\frac{d\alpha}{dT}\right)$ data.

$$RSS = min\sum_{i=1}^{n_d}\left[\left(\frac{d\alpha}{dT}\right)_{i,exp} - \left(\frac{d\alpha}{dT}\right)_{i,cal}\right]^2 \tag{11}$$

where n_d indicates the number of selected experimental data points, $\left(\frac{d\alpha}{dT}\right)_{i,exp}$ and $\left(\frac{d\alpha}{dT}\right)_{i,cal}$ denote the experimental and computed values of conversion rate, respectively, for a particular set of parameters. Given that the objective function does not have any explicit mathematical expression, the optimization problem is difficult to solve using conventional optimization techniques. Hence, a hybrid of the particle swarm optimization (PSO) [52], a widely-known metaheuristic optimization technique, and the pattern search (PS) [53] method was applied to solve Eq. (11). The hybrid PSO-PS algorithm was implemented in MATLAB®. The apparent reaction rate, $\left(\frac{d\alpha}{dT}\right)$, curves were generated by employing the estimated kinetic parameters of multi-DAEM and subsequently compared with ones acquired from TG experiments. To assess the model validity, a fitting parameter, as given by Eq. (12), was utilized [54].

$$Fit(\%)_{DTG} = \left(1 - \frac{\sqrt{\frac{S}{n_d}}}{\left(\frac{d\alpha}{dT}\right)_m}\right) \times 100\% \tag{12}$$

where $\left(\frac{d\alpha}{dT}\right)_m$ indicates the maximum recorded experimental value. The value of *Fit* in Eq. (12) expresses the discrepancies between the experimental DTG curves and those predicted by employing the multi-DAEM. A closer value of *Fit* to 100%, a higher fitting quality is achieved.

The model validity for conversion curves was assessed using the objective function (RSS^1), Eq. (13), and fitting parameter *Fit* (%)$_{\text{conv}}$, Eq. (14), which are analogous to Eqs. (11) and (12), respectively.

$$RSS^1 = min\sum_{i=1}^{n_d}\left[(\alpha)_{i,exp} - (\alpha)_{i,cal}\right]^2 \tag{13}$$

$$Fit(\%)_{conv.} = \left(1 - \sqrt{\frac{S^1}{n_d}}\right) \times 100\% \tag{14}$$

2.3.4. Discrete distributed activation energy model

The infinite reactions in DAEM can be discretized into numerous but finite independent parallel irreversible reactions. A discrete DAEM algorithm was presented in the study carried out by Scott et al. [35], where the activation energy was in the isoconversional form and could be evaluated utilizing thermogravimetric data at only two different constant heating rates. Accordingly, the infinite reactions are simplified by discretizing into N_r parallel first-order irreversible reactions, every of which follows its own characteristic activation energy and pre-exponential factor. For the pyrolysis process of PLP-PCBs, under linear non-isothermal conditions, the reaction rate of one such irreversible first-order reaction can be expressed as:

$$-\frac{dm_k}{dT} = \frac{A_k}{\beta_j}\exp\left(\frac{-E_k}{RT}\right)m_k \tag{15}$$

where m_k, E_k, and A_k are the instantaneous mass, the activation energy, and the pre-exponential factor of k^{th} reaction, respectively. The integral form of Eq. (15) is given by:

$$M_k = M_{k,0}exp\left[-\frac{A_k}{\beta_j}\psi(E_k,T)\right] \tag{16}$$

where $M_{k,0}$ and M_k represent the primary and instantaneous mass of the k^{th} reaction, respectively. The instantaneous mass of the sample is the sum of the mass of N_r reactions. Hence from Eqs. (15) and (16), the conversion function contributed by N_r number of first-order reactions throughout the pyrolysis process is expressed by:

$$x = 1 - \alpha = \frac{\sum_{k=1}^{N_d}M_k}{\sum_{k=1}^{N_d}M_{k,0}} - \sum_{i=1}^{N_r}w_{char,k} = \sum_{k=1}^{N_r}f_{k,0}exp\left[-\frac{A_k}{\beta_j}\psi(E_k,T_k)\right]$$
$$= \sum_{k=1}^{N_r}f_{k,0}\Phi_k(E_k,T_k) \tag{17}$$

where $f_{k,0}$ is the weight fraction contributed by k^{th} first-order reaction; N_r is the supposed number of first-order reactions; T_k is the corresponding temperature; β_j designates the j^{th} (j = 1, 2) heating rate; and $w_{char,k}$ represents the char mass fraction of the k^{th} reaction. Eq. (17) can be expressed linearly, as:

$$\underbrace{\begin{bmatrix} x(T_0)\\ x(T_1)\\ x(T_2)\\ .\\ .\\ . \end{bmatrix}}_{X} = \underbrace{\begin{bmatrix} \Phi_1(E_0,T_0) & \Phi_2(E_0,T_0) & \cdots & \Phi_{N_r}(E_0,T_0)\\ \Phi_1(E_1,T_1) & \Phi_2(E_1,T_1) & \cdots & \Phi_{N_r}(E_1,T_1)\\ \Phi_1(E_2,T_2) & \Phi_2(E_2,T_2) & \cdots & \Phi_{N_r}(E_2,T_2)\\ . & . & . & .\\ . & . & . & .\\ . & . & \cdots & . \end{bmatrix}}_{\Phi(E,T)} \times \underbrace{\begin{bmatrix} f_{1,0}\\ f_{2,0}\\ f_{3,0}\\ .\\ .\\ . \end{bmatrix}}_{f} \tag{18}$$

i.e. $\boldsymbol{X} = \boldsymbol{\Phi(E,T)} \times \boldsymbol{f}$, where $\boldsymbol{\Phi(E,T)}$ and $\boldsymbol{f}$ are in the matrix forms.

To calculate $f_{k,0}$ using Eq. (18), a set of reactions, each with a known value of E_k and A_k must first be generated. As an assumption, E_k and A_k assigned to a characteristic conversion degree are the same at various heating rates. Moreover, the k^{th} reaction is assumed to be the only reaction occurring at this extent of conversion. Therefore, one can conclude from Eq. (16):

$$\psi_k(E_k,T_1)|_{\beta_1} = \psi_k(E_k,T_2)|_{\beta_2} \tag{19}$$

i.e.

$$\frac{1}{\beta_1}\left[T_0\exp\left(\frac{-E_k}{RT_0}\right)-\frac{E_k}{R}\int_{\frac{E}{RT_0}}^{\infty}\frac{\exp(-u)}{u}du-T_1\exp\left(\frac{-E_k}{RT_1}\right)+\frac{E_k}{R}\int_{\frac{E}{RT_1}}^{\infty}\frac{\exp(-u)}{u}du\right]$$

$$=\frac{1}{\beta_2}\left[T_0\exp\left(\frac{-E_k}{RT_0}\right)-\frac{E_l}{R}\int_{\frac{E}{RT_0}}^{\infty}\frac{\exp(-u)}{u}du-T_2\exp\left(\frac{-E_i}{RT_2}\right)+\frac{E_k}{R}\int_{\frac{E}{RT_2}}^{\infty}\frac{\exp(-u)}{u}du\right] \quad (20)$$

where $u = E/(RT)$ and $T_{0,\beta 1}$ and $T_{0,\beta 2}$ denote the specified initial temperatures of β_1 and β_2, respectively. The activation energy of the k^{th} reaction (E_k) is calculated from Eq. (20). Once the E_k is obtained, assuming $x = 1 - e^{-1} \rightarrow \Phi(E_k, T) = e^{-1} \approx 36.8\%$, the pre-exponential factor A_k is computed by solving Eq. (21) under the given heating rates:

$$\ln \Phi(E_k,T) = -1 = \frac{A_k}{\beta_1}\left[T_0\exp\left(\frac{-E_k}{RT_0}\right)-\frac{E_k}{R}\int_{\frac{E_k}{RT_0}}^{\infty}\frac{\exp(-u)}{u}du-T_2\exp\left(\frac{-E_k}{RT_2}\right)+\frac{E_k}{R}\int_{\frac{E_k}{RT_2}}^{\infty}\frac{\exp(-u)}{u}du\right] \quad (21)$$

The value $\ln \Phi(E_k, T) = -1$ corresponds to the conversion at which an individual first-order reaction reaches the utmost weight loss rate at a constant heating rate. When A_k and E_k are known, the initial mass fractions ($f_{k,0}$) can be computed from Eq. (18) using the non-negative linear least-squares Method (NLLSM) with the following constraints:

$$\begin{cases} f_{k,0} \in [0\ 1] \\ \sum_{k=1}^{n} f_{k,0} = 1 \end{cases} \quad (22)$$

It is noteworthy that the main advantage of the discrete DAEMs over the PDF-based DAEMs is their relative ease of incorporation in comprehensive computational fluid dynamics (CFD) models extensively used for reactor design and process optimization. Coupling a PDF-based DAEM with the CFD calculations is computationally expensive due to the requirement of multiple improper numerical integrations for every computational cell at each time step [55,56]. Given that no simplification and multiple numerical integrations are required, incorporating the discrete DAEMs in a CFD program would lead to much more accurate simulation results with significantly lower computational costs, compared to the CFD models with the PDF-based DAEMs.

3. Results and discussion

3.1. TGA thermal behavior

3.1.1. Pyrolysis characteristics

TG-DTG analyses were implemented to appraise the pyrolysis behavior of PLP-PCB. Fig. 1 exhibits the mass loss (%) profile and derivative mass loss (% min^{-1}) curve throughout the pyrolysis process of PLP-PCB under an N_2 atmosphere at a constant linear heating rate of 10 °C min^{-1} in the temperature range from 25 to 800 °C. The TG-DTG curves provide valuable information about the thermo-physical features of the PLP-PCB. The pyrolysis characteristics of PLP-PCB are tabulated in Table S2. From ambient temperature to -150 °C, approximately 2% weight loss was detected, mainly due to the elimination of moisture that is present within the samples and/or bounded by surface tension. The main pyrolytic process proceeded in a wide temperature region from -150 to -520 °C, representing an appreciable weight loss percentage (= 88 wt.% of the overall mass loss) generally regarded as the devolatilization stage. The pyrolysis behavior in this temperature zone was particularly complex as evidenced by the multiple overlapping peaks and shoulders on the DTG curve. As seen in Fig. 1, in this region, two shoulder-shaped peaks and two pronounced peaks could be identified, characteristics of which are listed in Table S2. At elevated temperatures (above ~550 °C), the pyrolytic behavior was characterized by minor mass losses, probably associated with the degradation of carbonaceous materials preserved in char residues. This stage accounted for about 8.4 wt.% of the overall mass loss. The drying stage ($T < 150$ °C) was excluded from the pyrolysis analysis, as the primary focus of the present research is the thermal degradation process.

According to the nature of curves and variations in the mass loss rate, as illustrated in Fig. 1, the reduction in the mass of samples during the devolatilization stage can be observed in four distinct phases, which can be described by the various reaction stages taking place throughout the thermal decomposition of PLP-PCB, as reported in the literature. The temperature regions of the main decomposition phases are listed in Table S3. The first step is Stage I, spanning from 151 to 244 °C, which is characterized by a vivid left shoulder at about 240 °C on the DTG curve and is primarily attributed to the evaporation of phosphorous-based flame retardants [29]. The second phase (Stage II) manifests a significant mass loss and encompasses a broad temperature range, approximately extending from 244 to 348 °C, which is denoted by the pronounced peak at 311.4 °C with a maximum mass loss rate of 0.0011% s^{-1} and could be mainly ascribed to the thermal degradation of laminated paper and tetrabromobisphenol A (TBBA) [57]. The third step is

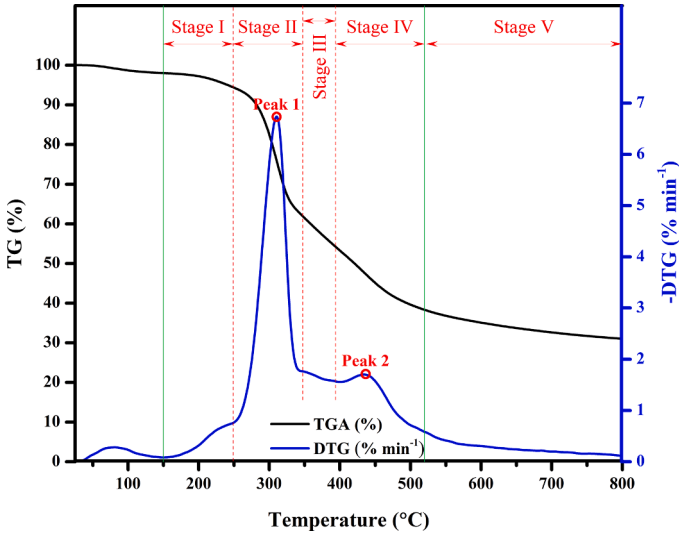

Fig. 1. TG/DTG curve of PLP-PCB pyrolysis under a heating rate of 10 °C min^{-1}.

Stage III, ranging from 348 to 395 °C, which is characterized by a right shoulder at approximately 350 °C on the DTG curve. The fourth part is Stage IV, taking place between temperatures 395 to 521 °C. The corresponding region on the DTG profile is rendered by the peak located at 435.5 °C with a maximum mass reduction rate of 0.0003% s^{1}. Stages III and IV mostly appertain to the pyrolysis of phenol resin [28]. The completion of the PLP-PCB pyrolysis process was around 550 °C, leaving almost 31 wt.% remnants upon further heating, which is in accordance with the total of the fixed carbon and ash contents measured by the proximate analysis. The TG-DTG analysis allows for determining the temperature limits for the various decomposition phases, which could subsequently be coupled with the kinetic estimations to gain a better understanding of the PLP-PCB pyrolysis reaction mechanism.

3.1.2. Effect of heating rate

The heating rate wields a considerable influence on the pyrolysis characteristics [58]. More specifically, it can alter the TG-DTG curve shape and the pyrolysis characteristic temperatures. TG analysis of the PLP-PCB sample was conducted at four different heating rates of 10, 15, 20, and 30 °C min^{-1}. The acquired TG-DTG profiles are exhibited in Fig. 2 to examine the effect of varying heating rates over the non-isothermal kinetics. As illustrated in Fig. 2, the higher heating rates afford a shift in both TG and DTG profiles toward the upper-temperature regions, with different expanses depending upon the heating rate. This signifies that for a higher heating rate, an elevated temperature is required to initiate the devolatilization process. It is evident from Fig. 2 that the patterns of TG-DTG graphs at various heating rates are pretty much analogous, implying that the pyrolysis mechanism within the considered temperature range is mostly unaffected by variations in the heating rate [59]. As a means to quantitatively describe the features of the PLP-PCB pyrolysis process under the influence of varied heating rates, several characteristic parameters computed from the TG-DTG diagrams are provided in Tables S2 and S3.

The impact of the heating rate on the characteristic temperatures of pyrolysis is predominantly ascribed to the restricted rate of heat conduction within the sample particles caused by thermal resistance. As the heating rate rises, the time duration taken to reach the decreed final temperature over the same temperature range diminishes. Hence, the total heat transferred from the heating furnace to the test sample within the thermogravimetric apparatus is restricted. Consequently, temperature gradients might form within the particles as a result of the heat conduction limitations, which may arise discrepancies between the recorded and actual sample temperatures. Due to the enhanced supply of thermal energy per unit of time at the higher heating rates, an intensified thermal decomposition rate is achieved in view of the general endothermicity of the pyrolysis reactions.

Similar shifts in the characteristic temperatures, as well as the enhancement in the decomposition rates with rising the heating rate, were also reported by Chen et al. [60] and Yao et al. [61] for the pyrolysis of WPCBs in an inert environment.

3.2. Kinetic models

3.2.1. Iso-conversional methods

The decomposition kinetics during the PLP-PCB pyrolysis process is investigated within the conversion degree (α) of 0.05–0.95 with a step-size of 0.05 by applying three isoconversional model-free methods, including FWO and KAS integral methods, and the Friedman differential method. The kinetic parameters were evaluated via plotting $\ln(\beta_i)$, $\ln(\beta_i/T_{\alpha,i}^2)$, and $\ln(\beta_i(d\alpha/dT)_{\alpha,i})$ against $1/T_{\alpha,i}$ for the FWO, KAS, and Friedman approaches, respectively, using TG datasets from four different heating rates. The isoconversional linear fitting diagrams issued from all the employed model-free methods are depicted in Fig. 3(a-c). The apparent activation energies (E_α) and the pre-exponential factors (A_α), within the considered conversion range, were computed from the slopes and the intercepts of the isoconversional straight lines. The coefficient of determination (R^2) was employed as the performance metrics to assess the quality of the fitted lines. Table 2 lists the acquired kinetic parameters and corresponding R^2 values at various conversions for FWO, KAS, and Friedman methods. While the activation energy range obtained from the Friedman method was within 117.91–617.53 kJ mol^{-1}, the FWO and KAS methods demonstrate a rather similar range of 138.16–583.61 kJ mol^{-1} and 137.08–599.81 kJ mol^{-1}, respectively. The average apparent activation energy (E_{ave}) of PLP-PCB pyrolysis estimated from the different isoconversional methods applied varied between 262.82 and 279.45 kJ mol^{-1}. Regardless of the model, the coefficients of determination of the obtained E_α were close to unity, indicating the capability of the tested models for estimation of the PLP-PCB kinetics. The lower R^2 values at high conversions ($\alpha \geq 0.9$) could be ascribed to the slow secondary reactions, the occurrence of multi-step reactions, the catalytic effects of associated metals, and non-uniform diffusion [62]. To further investigate the kinetic parameters derived from the different methods, the values of $\ln(A_\alpha)$ were plotted against E_α. As depicted in Fig. 3(d), for all methods, $\ln(A_\alpha)$ varies almost linearly with E_α, indicating the dominance of the kinetic compensation effect (KCE). The KCE states that a rise in E_α, which is equivalent to a decrease in the rate of reaction at a given temperature, is partially or completely compensated by an increase in A_α [63]. The obtained compensation

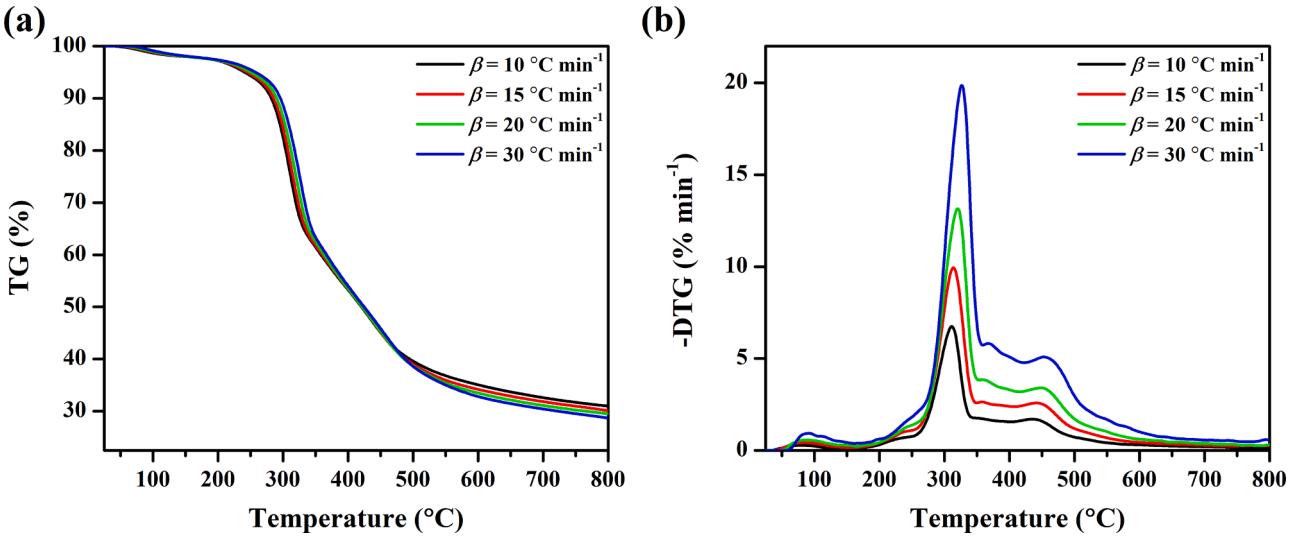

Fig. 2. (a) TG and (b) DTG profiles of PLP-PCB under various heating rates of 10–30 °C min^{-1}.

Table 2
Kinetic parameters of PLP-PCB pyrolysis derived from Friedman, FWO, and KAS methods at different conversion levels.

Conversion (%)	Friedman			FWO			KAS		
	E_α (kJ mol^{-1})	ln(A_α) (s^{-1})	R^2	E_α (kJ mol^{-1})	ln(A_α) (s^{-1})	R^2	E_α (kJ mol^{-1})	ln(A_α) (s^{-1})	R^2
5	117.91	20.03	0.997	138.16	26.59	0.990	137.08	26.27	0.988
10	179.68	32.07	1.000	149.26	26.65	0.998	147.94	26.30	0.998
15	211.44	38.61	0.999	185.79	33.96	0.999	186.08	34.00	0.999
20	210.42	38.12	0.998	198.00	36.24	0.999	198.77	36.37	0.999
25	205.49	36.85	0.999	201.54	36.73	0.999	202.38	36.87	0.999
30	202.57	36.00	0.999	202.02	36.61	0.999	202.78	36.73	0.999
35	202.23	35.68	1.000	201.89	36.37	0.999	202.56	36.48	0.999
40	202.63	35.44	1.000	201.89	36.16	1.000	202.47	36.24	1.000
45	202.64	34.91	1.000	202.01	35.91	1.000	202.50	35.98	1.000
50	200.29	33.37	1.000	201.55	35.35	1.000	201.87	35.39	1.000
55	235.38	38.71	0.998	212.54	36.54	1.000	213.15	36.63	1.000
60	270.52	43.96	0.995	245.25	41.66	0.997	247.24	41.98	0.997
65	298.65	47.53	0.991	277.01	46.20	0.993	280.31	46.70	0.993
70	305.30	47.10	0.987	296.18	48.12	0.989	300.11	48.69	0.988
75	299.68	44.79	0.990	296.68	46.71	0.990	300.28	47.22	0.989
80	321.34	47.06	0.984	303.45	46.50	0.988	307.05	46.99	0.987
85	431.72	62.64	0.959	368.50	55.52	0.970	375.04	56.34	0.968
90	594.06	82.88	0.822	528.96	77.14	0.845	543.08	78.58	0.834
95	617.53	81.57	0.814	583.60	81.02	0.847	599.81	82.54	0.836
Average (±SE)	279.446 (±29.89)	44.07(±3.56)		262.86 (±26.46)	43.16 (±3.25)		265.82 (±27.51)	43.49 (±3.36)	

effect equations shown in Fig. 3d are similar to those reported by Hu et al. [31] and Yao et al. [64].

Fig. 4 depicts the apparent E_a distribution against α for FWO, KAS, and Friedman methods. As understood from Fig. 4, the activation energy profiles computed by all three isoconversional methods are quite comparable, therefore, they all are capable of providing a conceptual basis for the analysis of the PLP-PCB pyrolysis process. It is noticeable, however, that the E_a values obtained from the Friedman differential approach are marginally higher compared to those obtained from the isoconversional integral methods. Except for the Friedman method, other methods incorporate assumptions and some approximations in the course of solving the model's formulation. The Friedman method adopts the simple differential formulation of the kinetic rate equation (Eq. (4)) and involves no simplistic approximation to evaluate the temperature function. This may explain the minor discrepancies observed between the E_a values obtained from the Friedman method and the isoconversional integral methods. It should be remarked that the dependence of the Friedman method on the instantaneous conversion rate makes it more prone to measurement noises. Since the KAS method has been reported to provide more accurate E_α values when compared with FWO [65], this method was chosen to study the thermal decomposition mechanism in the following sections.

The variation trend of the apparent E_α with the increment of α is correlated with the reaction stages demarcated by the TG-DTG analysis. As illustrated in Fig. 4, the fluctuation pattern of E_α for the PLP-PCB pyrolysis can be roughly partitioned into five distinct regions corresponding to five main stages of the TG-DTG curves, i.e. Stage I (α = 0.05–0.075), Stage II (α = 0.075–0.55), Stage III (α = 0.55–0.70), Stage IV (α = 0.70–0.85), and Stage V (α = 0.85–0.95). At the end of Stage I (α = 0.075), the apparent activation energy is 142.5 kJ mol^{-1}. In Stage II, the E_α rises to 202.4 kJ mol^{-1} (α = 0.25) and then exhibits a stable profile within a broad conversion range ($0.3 < \alpha < 0.55$) with E_α around 204.2 kJ mol^{-1}, followed by a steady increase to 300.1 kJ mol^{-1} (α = 0.70) at Stage III. In Stage IV, the E_α increases from 300.1 to 375 kJ mol^{-1} when α ranges from 0.70 to 0.85. Finally, Stage V displays a rapid ascent of E_α values to 599.8 kJ mol^{-1} (α = 0.95), which explains the observed diminution of the reaction rate at these conversion levels inferred from very low values of the DTG curves at this stage. A similar variation pattern for activation energy was also reported by Kim et al. [57] with minor dissimilarities, which are attributed to the inherent differences in the structural characteristics of the studied PLP-PCBs. The activation energy, by definition, is the minimum required energy level to initiate a chemical reaction and could also be considered a potential measure for the reactivity of a component [66]. The significant variations in E_a distributions generally reflect the heterogeneous nature of PLP-PCBs, leading to complicated multi-stage reaction schemes involving parallel, competitive, and consecutive reactions [67]. Additionally, possible secondary reactions may play a prominent role during thermal degradation, influencing the kinetic pathway and thus the E_α values [68].

As referred to earlier, the isoconversional approaches were formulated from the one-step global reaction kinetics and might not be the preferable choice to describe a process involving multiple reactions, therefore, a more elaborate model is necessary for a better prediction. However, Vyazovkin et al. [40] recommended that the acquired kinetic parameters from the isoconversional model-free methods are desirable for making an initial guess at the model-fitting kinetic models.

3.2.2. Gaussian DAEM kinetics

To provide a more accurate understanding of the PLP-PCB pyrolysis kinetics, distributed activation energy models (DAEMs) were developed. The kinetic parameters were evaluated by employing the DTG measurements acquired at 10 and 30 °C min^{-1}. By applying the same parameters, the pyrolytic behavior at 15 and 20 °C min^{-1} was predicted and then compared with the corresponding experimental data. As outlined in Section 3.2.1, five reaction steps occur throughout the thermal degradation process of PLP-PCB. Therefore, in the first modeling approach, a five pseudo-component Gaussian DAEM was applied to mathematically describe the pyrolysis kinetics of the PLP-PCB. However, the thermal behavior simulated using this model did not adequately agree with the experimental data. Hence, one more pseudo-component was considered in the multi-Gaussian DAEM. Table 3 reports the optimized set of the kinetic parameters that best represent the experimental results. The mean activation energies (E_0) for PLP-PCB vary in the range of 149.46–479.30 kJ mol^{-1}. The calculated values for pre-exponential factors lie in the range of 4.91×10^{12} to 1.37×10^{26} s^{-1}, which is reasonable considering transition-state theory [54].

The Gaussian activation energy distribution curves, $f(E)$, for PLP-PCB pyrolysis are shown in Fig. 5. The narrowest spread for the activation energy distribution was observed for the 2nd pseudo-component (σ_{E2} = 2.31 kJ mol^{-1}), while the widest spread was noticed for the 6th pseudo-component (σ_{E6} = 48.89 kJ mol^{-1}). Moreover, one minor peak appeared as the 3rd pseudo-component as its fraction was tiny (c_3 = 0.04), the smallest one relative to other pseudo-components. This indicates one minor reaction that could not have been detected in the isoconversional kinetic study. The sum of all the Gaussian distribution peaks in Fig. 5 is

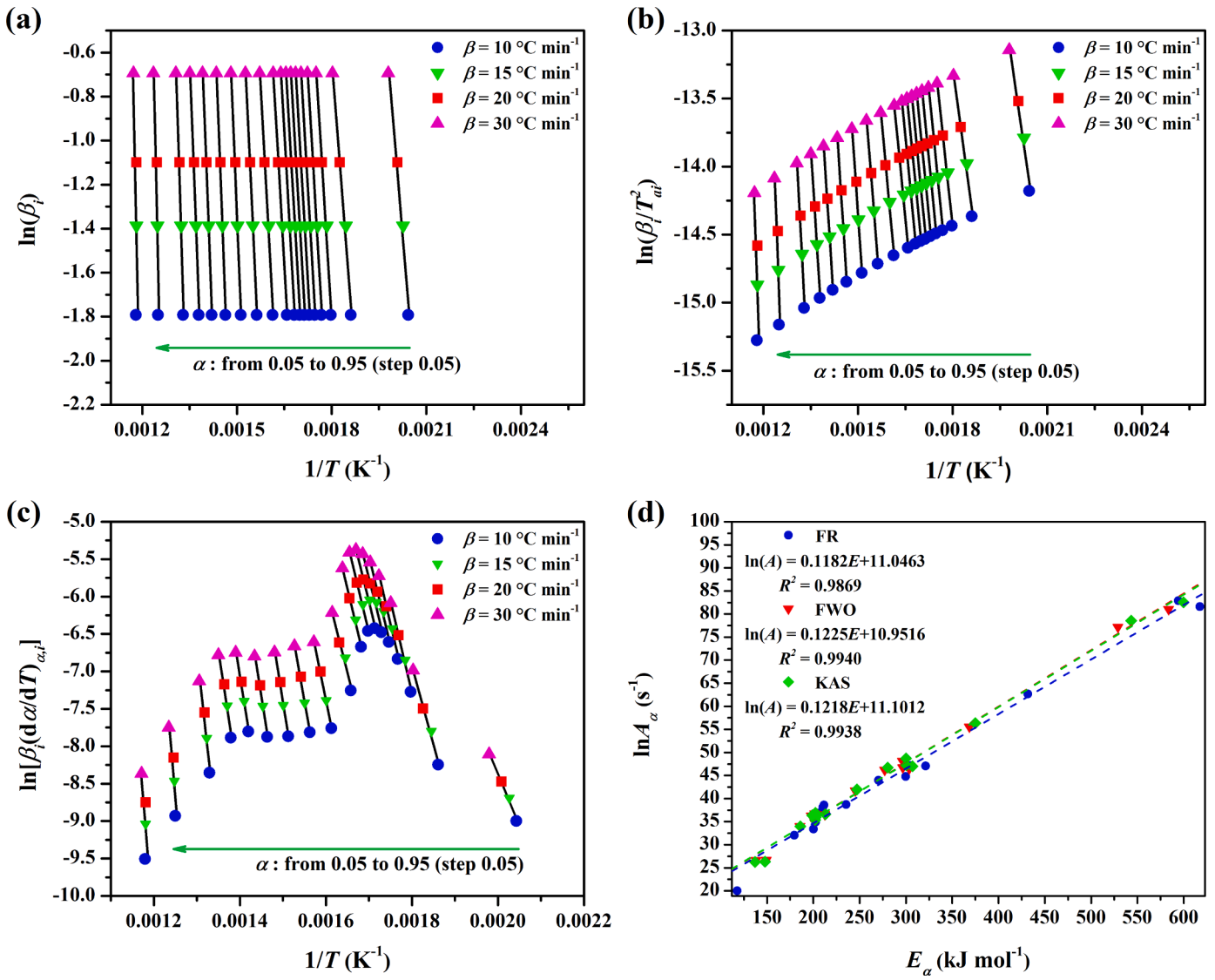

Fig. 3. Iso-conversional lines derived from (a) FWO, (b) KAS, and (c) Friedman method at selected degrees of conversion for PLP-PCB pyrolysis using TGA data during different heating rates; (d) linear fit plots for the compensation effects between the pre-exponential factor (A_α) and the activation energy (E_α) as obtained from the Friedman, KAS and FWO methods.

denoted by "*PeakSum*", representing the distribution of the activation energies over the entire reaction regime. Given that about 99.7% of the values taken from a normal distribution lie within three standard deviations ($3\sigma_E$) away from the mean, the activation energies calculated from '$E_0 \pm 3\sigma_E$' falls in the range of 109.83 to 625.97 kJ mol^{-1}.

Fig. 6 compares the experimental conversion rates as well as the conversion degree profiles with those predicted by the multi-Gaussian DAEM at four tested heating rates. As seen, the model-predicted curves are in excellent agreement with the experimental data, demonstrating an accurate interpretation of the pyrolysis process of PLP-PCB. The calculated *Fit* values for the conversion rate profiles were >96%, while those for the conversion degree profiles were >97%, authenticating the assumption of taking six pseudo-components into account.

According to the multi-Gaussian distribution model, the thermal decomposition regimes of pseudo-components are 150–330 °C, 230–350 °C, 290–380 °C, 270–470 °C, 330–540 °C, and 500–800 °C, respectively. The pseudo-component P1 describes the vaporization of phosphorus-based flame retardants evaporating at about 200 °C through a single-stage weight loss [69].

The pseudo-component P2 represents the decomposition of laminated paper and TBBA. The average activation energy at this stage was 198.03 kJ mol^{-1}, which is similar to that of cellulose decomposition (198 kJ mol^{-1}) [70], implying the trivial impact of TBBA on the kinetics of PLP-PCB degradation due to its low quantities in the samples tested in this work (cf. Table S1). White et al. [71] found that the thermal degradation of cellulose at this temperature range (280–350 °C) occurs through a different reaction pathway relative to that assessed at lower temperatures. In particular, the predominant depolymerization reaction occurring in this temperature range is the breakage of the β−1, 4-glycosidic linkages, producing a tarry pyrolyzate comprising levoglucosan, other anhydrospamics, oligosaccharides, and some glucose degradation products.

The pseudo-components P3, P4, and P5 consider a wide variety of compounds formed during the pyrolysis of phenolic resins. At the initial part of this stage, the breakage of the bonds linking the benzene rings and the scission of ether bonds predominate [72,73]. With further increase in the temperature, the benzene rings undergo a dehydrogenation reaction and gradually fuse, leading to the formation of a graphitic carbon structure with a higher level of activation energy [74]. Jiang et al. [75] reported that the thermal decomposition process of phenolic resins is comprised of three consecutive and overlapped reaction stages with the mean activation energies of 222.73, 271.70, and 305.14 kJ

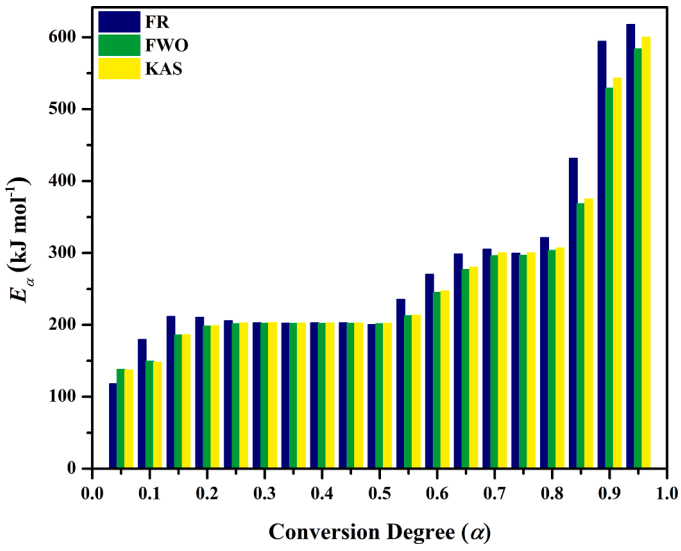

Fig. 4. Variation of the apparent activation energy with the extent of conversion for PLP-PCB pyrolysis process computed by Friedman, FWO, and KAS methods.

Table 3
Optimized kinetic parameters of six pseudo-components for thermal decomposition of PLP-PCB samples obtained from the Gaussian DAEM kinetics. .

Pseudo-component	c_j	A (s^{-1})	E_0 (kJ mol^{-1})	σ_E (kJ mol^{-1})
P1	0.12	4.91×10^{12}	149.46	13.21
P2	0.37	5.89×10^{15}	198.03	2.31
P3	0.04	6.71×10^{18}	248.92	3.56
P4	0.13	4.69×10^{19}	269.94	13.64
P5	0.20	7.19×10^{20}	315.02	16.77
P6	0.14	1.37×10^{26}	479.30	48.89

mol^{-1}, which are consistent with the values estimated in this study.

The degradation of carbonaceous substances in char is represented by the sixth pseudo-component (P6). The multi-Gaussian DAEM provides accurate estimates for kinetic parameters of the PLP-PCB pyrolysis, which are crucial for a profound understanding of the thermal decomposition process and for developing precise models with far-reaching applications in the modeling suites of the pyrolysis process.

3.2.3. Discrete DAEM kinetics

In the present study, the PLP-PCB pyrolysis process was discretized into $N_r = 97$ first-order parallel reactions, each corresponding to a characteristic conversion degree (α) in the range of 0.03–0.99 with a step-size of 0.01. Thermogravimetric datasets of two different heating rates (10 and 30 °C min^{-1}) were adopted to compute E_k values at each conversion degree by solving Eq. (20). The values of A_k were estimated by substituting E_k values into Eq. (21). Once E_k and A_k have been acquired, the initial mass fraction ($f_{k,0}$) of any given reaction was estimated from Eq. (18) via the non-negative linear least-squares method (NLLSM) with constraints of Eq. (22).

Fig. 7 depicts the values of the activation energy and the associated pre-exponential factor for the conversion degree ranging from 0.03 to 0.99, as obtained from the discrete DAEM algorithm applied to the TG measurements. The fluctuation trend of the activation energy versus the extent of conversion (α) is complex. As illustrated in Fig. 7, the E_k values initially rose from 107.8 to 201.9 kJ mol^{-1} for α ranging from 0.03 to 0.27, followed by an almost constant profile over a wide range of α (0.27–0.52). After a slight decline in the E_k values for α values ranging from 0.72 to 0.75, a sharp climb to $E_k = 601.1$ kJ mol^{-1} was noticed at $\alpha = 0.95$. Finally, the E_k values declined considerably to 334.2 kJ mol^{-1} for $0.95 < \alpha < 0.99$. The reduction in E_k in the range of 0.72 to 0.75 was possibly due to the formation of a small amount of slightly porous char. The enhanced diffusion in the porous char can explain the reduction in the apparent activation energy [76]. The decrement of E_k in the range of 0.95 to 0.99 can be explained in light of the formation of high quantities of porous char, as well as the in-situ catalytic effect of the alkali metals existing in the reinforcing materials contained in the samples. These effects are particularly pronounced at high conversion levels (or temperatures) [77,78].

The dependency of E_k on α can be exploited to identify the variation of decomposition mechanisms. The $\ln(A_k)$ values increase from 21.84 to 36.94 s^{-1}, from 35.27 to 48.12 s^{-1}, and from 46.23 to 78 s^{-1} when α ranges from 0.03 to 0.24, from 0.53 to 0.70, and from 0.79 to 0.95, respectively. However, an opposite tendency was detected when α

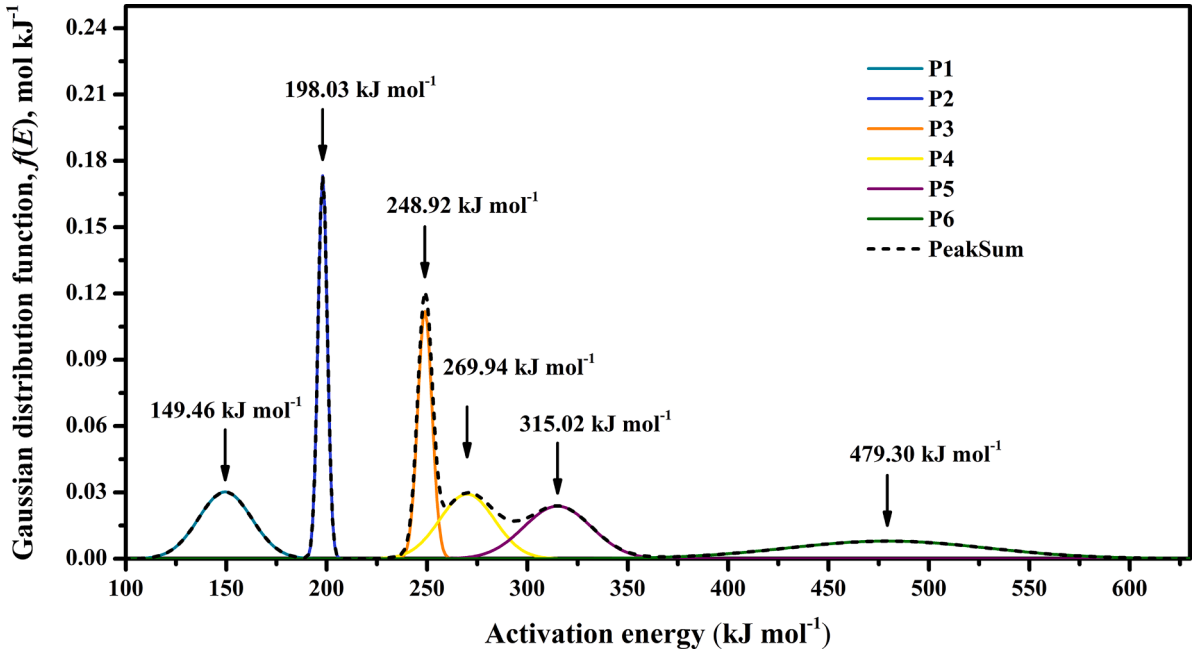

Fig. 5. The Gaussian distribution of the activation energy of six pseudo-components involved in the PLP-PCB pyrolysis.

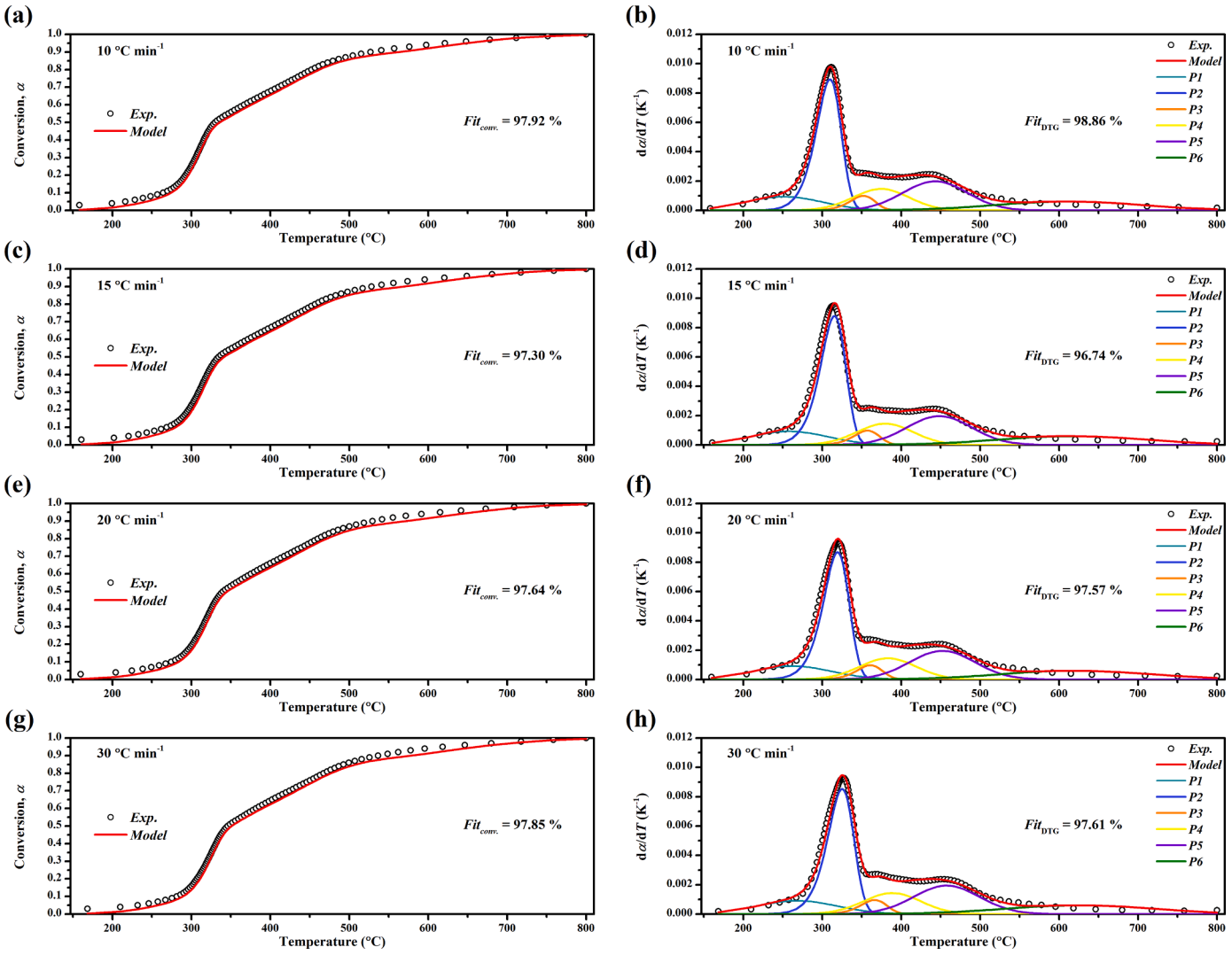

Fig. 6. Comparison between the TG-DTG results and the data predicted by the multi-Gaussian DAEM at different heating rates.

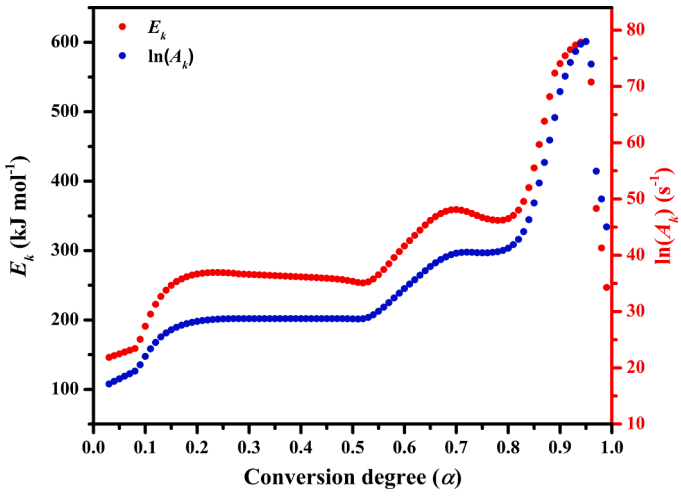

Fig. 7. Kinetic parameters obtained from applying the discrete DAEM algorithm to the pyrolysis of PLP-PCB.

ranges from 0.25 to 0.52, from 0.71 to 0.78, and from 0.96 to 0.99, wherein the $\ln(A_k)$ values decrease from 36.91 to 35.07 s^{-1}, from 48.01 to 46.19 s^{-1}, and from 70.79 to 34.27 s^{-1}, respectively. As evidenced by Fig. 7, the distributions of E_k and $\ln(A_k)$ vs. the extent of conversion follow a very similar variation trend denoting the satisfaction of the "kinetic compensation effect".

The distribution of the initial mass fraction with the conversion degree is shown in Fig. 8. The majority of 97 first-order parallel reactions postulated by the discrete DAEM algorithm have non-effective contributions to the pyrolysis process since, as seen in Fig. 8, their corresponding $f_{k,0}$ is zero. Conversely, the 37 reactions with $f_{k,0} \neq 0$ contribute to the pyrolysis process, and the larger the $f_{k,0}$ value of a reaction, the greater its contribution to the process. As demonstrated in Fig. 8, by taking the $d\alpha/dT$ vs. α curve as a reference, the distribution of $f_{k,0}$ could be divided into five stages. The first stage occurred at α of 0.03–0.075 and had a mean activation energy (E_0) of 113.87 kJ mol^{-1}, which was ascribed to the evaporation of phosphorus-based flame retardants [29]. The second stage took place at the conversion range of 0.075–0.55, with a mean activation energy of 195.87 kJ mol^{-1}. Such a stage was primarily ascribed to laminated paper pyrolysis [57], which encompasses the top three dominating reactions at conversions 0.24, 0.23, and 0.12 with the corresponding $f_{k,0}$ values of 0.23, 0.09, and 0.07, respectively. The third and fourth stages were located at α ranges of 0.55–0.68 and 0.69–0.87 with mean activation energies of 245.89 and

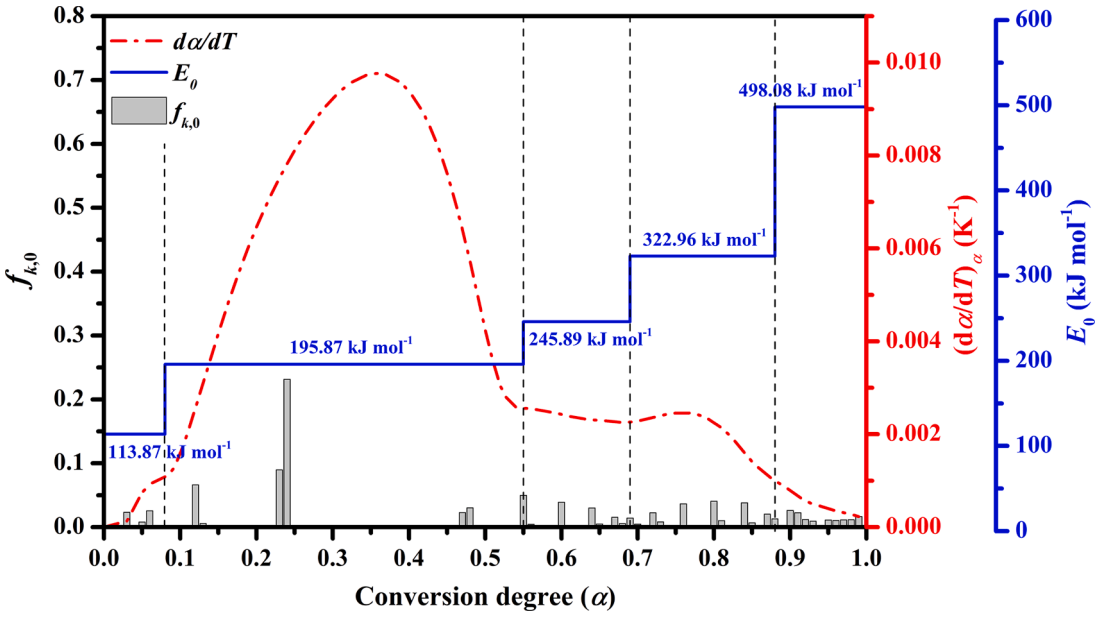

Fig. 8. Initial mass fractions distribution allied with the conversion rate curve and mean activation energies.

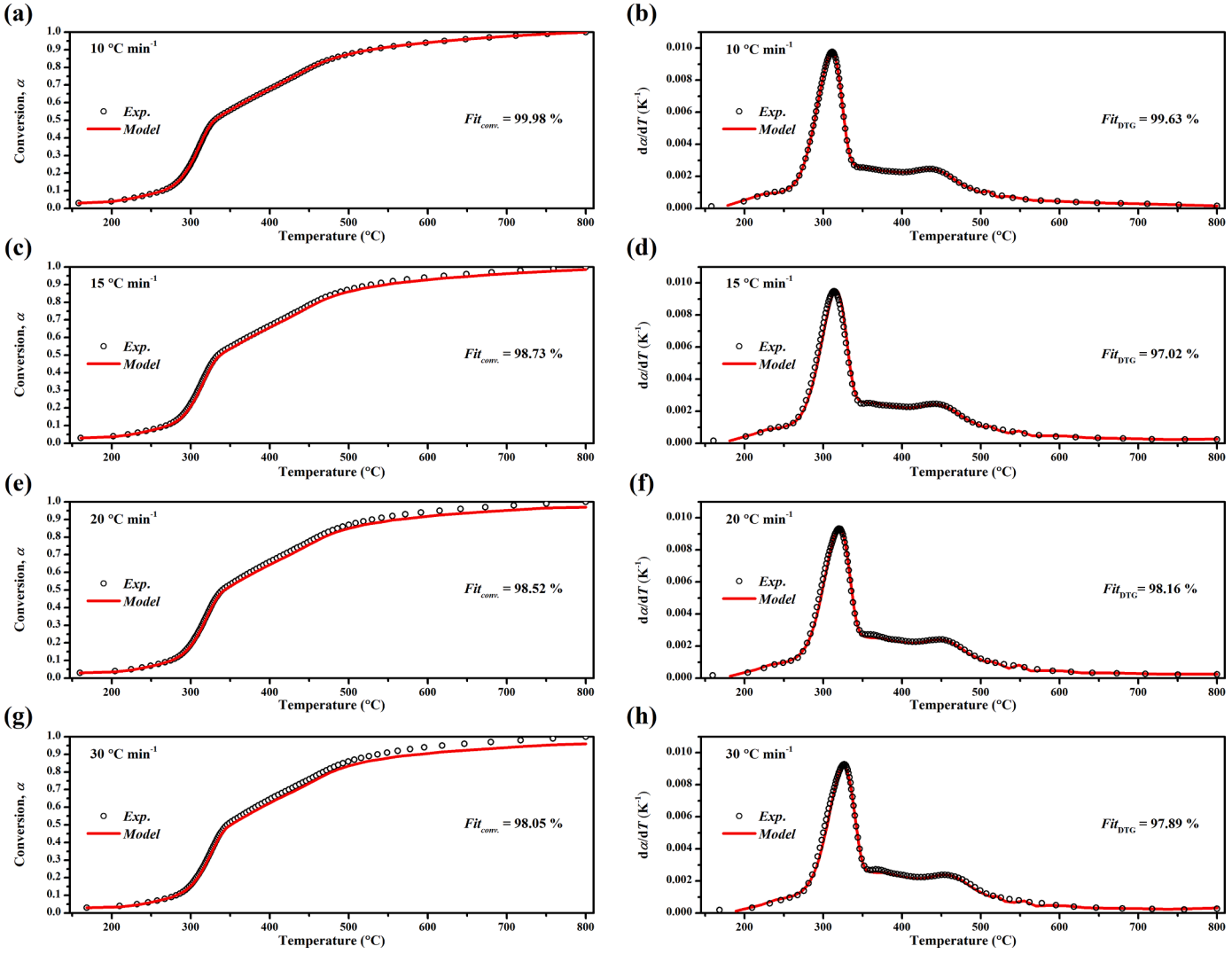

Fig. 9. Comparison between the TG-DTG results and the data predicted by the discrete DAEM algorithm at different heating rates.

322.96 kJ mol^{-1}, respectively, which were imputed to the thermal decomposition of phenol resin [28]. The fifth stage represented the tail of the DTG diagram and occurred at elevated conversions (or temperatures). The mean activation energy of this stage was calculated to be 498.08 kJ mol^{-1}. The apparent pre-exponential factors and activation energies of these five reaction stages are in excellent agreement with those obtained in Sections 3.2.1 and 3.2.2.

Fig. 9 compares the experimental conversion rates and the conversion degree plots with those predicted by the discrete DAEM at heating rates of 10, 15, 20, and 30 °C min^{-1}. The *Fit* values were >97% for all conversion rate diagrams and conversion degree curves, indicating the capability of the model for providing an accurate description of the kinetic behavior of PLP-PCB pyrolysis.

4. Conclusions

In the present investigation, the pyrolysis of PLP-PCB was studied utilizing non-isothermal thermogravimetric analysis. Three isoconversional kinetic models (including Friedman, FWO, and KAS) were employed for the initial evaluation and analysis of the pyrolysis mechanism. The variation pattern of the calculated activation energies throughout the pyrolysis process was addressed in detail. Furthermore, by assuming the occurrence of parallel first-order irreversible reactions, both multi-Gaussian and discrete distributed activation energy models (DAEM) have been developed to simulate the thermal degradation behavior of PLP-PCB during the pyrolysis process. The pyrolytic kinetics of PLP-PCB was accurately described by the Gaussian DAEM based on six pseudo-components. The mean activation energy for these pseudo-components were 149.49, 198.03, 248.92, 269.94, 315.02, and 479.30 kJ mol^{-1}, with the standard deviations of 13.21, 2.31, 3.56, 13.64, 16.77, and 48.89 kJ mol^{-1}, and the pre-exponential factors of 4.91×10^{12}, 5.89×10^{15}, 6.71×10^{18}, 4.69×10^{19}, 7.19×10^{20}, and 1.37×10^{26} s^{-1}, respectively.

According to the discrete DAEM, the pyrolysis process of PLP-PCB could be accurately modeled by 37 dominating first-order reactions with the apparent activation energies ranging from 107.8 to 601.1 kJ mol^{-1} and the pre-exponential factors ranging from 3.06×10^{9} to 7.50×10^{33} s^{-1}. The DAEMs with multi-Gaussian and discrete distributions were capable to predict both conversion and conversion rate profiles very accurately.

The results obtained in this research can be exploited to design, simulate, and control the pyrolyzers involving PLP-PCBs. However, for a specific type of pyrolyzer, it is advised to derive the pyrolysis kinetics by taking the pertinent hydrodynamic, heat, and mass transfer phenomena into account. Moreover, a more detailed kinetic model would be useful to shed light on the secondary reactions such as the cracking of the formed volatiles.

Declaration of Competing Interest

The authors declare that they have no known competing financial interests or personal relationships that could have appeared to influence the work reported in this paper.

Data availability

Data will be made available on request.

Supplementary materials

Supplementary material associated with this article can be found, in the online version, at doi:10.1016/j.tca.2023.179513.

References

[1] Forti, V., Baldé, C.P., Kuehr, R., Bel, G. The Global E-waste Monitor (GEM) 2020 – Quantities, flows, and the circular economy potential. http://ewastemonitor.info/gem-2020.
[2] A. Kumar, M.E. Holuszko, T. Janke, Characterization of the non-metal fraction of the processed waste printed circuit boards, Waste Manag. 75 (2018) 94–102, https://doi.org/10.1016/j.wasman.2018.02.010.
[3] Y. Zhou, K. Qiu, A new technology for recycling materials from waste printed circuit boards, J. Hazard. Mater. 175 (2010) 823–828, https://doi.org/10.1016/j.jhazmat.2009.10.083.
[4] J. Guo, J. Guo, Z. Xu, Recycling of non-metallic fractions from waste printed circuit boards: a review, J. Hazard. Mater. 168 (2009) 567–590, https://doi.org/10.1016/j.jhazmat.2009.02.104.
[5] J.A. Salbidegoitia, E.G. Fuentes-Ordóñez, M.P. González-Marcos, J.R. González-Velasco, T. Bhaskar, T. Kamo, Steam gasification of printed circuit board from e-waste: effect of coexisting nickel to hydrogen production, Fuel Process. Technol. 133 (2015) 69–74, https://doi.org/10.1016/j.fuproc.2015.01.006.
[6] W. Liu, J. Xu, J. Han, F. Jiao, W. Qin, Z. Li, Kinetic and mechanism studies on pyrolysis of printed circuit boards in the absence and presence of copper, ACS Sustain. Chem. Eng. 7 (2019) 1879–1889, https://doi.org/10.1021/acssuschemeng.8b03382.
[7] L. Rocchetti, A. Amato, F. Beolchini, Printed circuit board recycling: a patent review, J. Clean. Prod. 178 (2018) 814–832, https://doi.org/10.1016/j.jclepro.2018.01.076.
[8] R. Wang, Z. Zhu, S. Tan, J. Guo, Z. Xu, Mechanochemical degradation of brominated flame retardants in waste printed circuit boards by Ball Milling, J. Hazard. Mater. 385 (2020), 121509, https://doi.org/10.1016/j.jhazmat.2019.121509.
[9] A. Anindya, D.R. Swinbourne, M.A. Reuter, R.W. Matusewicz, Distribution of elements between copper and FeO x –CaO–SiO 2 slags during pyrometallurgical processing of WEEE, Miner. Process. Extr. Metall. 122 (2013) 165–173, https://doi.org/10.1179/1743285513Y.0000000043.
[10] M. Arshadi, S. Yaghmaei, S.M. Mousavi, Content evaluation of different waste PCBs to enhance basic metals recycling, Resour. Conserv. Recycl. 139 (2018) 298–306, https://doi.org/10.1016/j.resconrec.2018.08.013.
[11] X. Guo, J. Liu, Optimization of low-temperature alkaline smelting process of crushed metal enrichment originated from waste printed circuit boards, J. Cent. South Univ. 22 (2015) 1643–1650, https://doi.org/10.1007/s11771-015-2682-8.
[12] A.B. Sodha, D.R. Tipre, S.R. Dave, Optimisation of biohydrometallurgical batch reactor process for copper extraction and recovery from non-pulverized waste printed circuit boards, Hydrometallurgy 191 (2020), 105170, https://doi.org/10.1016/j.hydromet.2019.105170.
[13] T. Moyo, B... Chirume, J. Petersen, Assessing alternative pre-treatment methods to promote metal recovery in the leaching of printed circuit boards, Resour. Conserv. Recycl. 152 (2020), 104545, https://doi.org/10.1016/j.resconrec.2019.104545.
[14] J. Hao, H. Wang, S. Chen, B. Cai, L. Ge, W. Xia, Pyrolysis characteristics of the mixture of printed circuit board scraps and coal powder, Waste Manag. 34 (2014) 1763–1769, https://doi.org/10.1016/j.wasman.2013.10.043.
[15] J. Sun, W. Wang, Z. Liu, Q. Ma, C. Zhao, C. Ma, Kinetic study of the pyrolysis of waste printed circuit boards subject to conventional and microwave heating, Energies 5 (2012) 3295–3306, https://doi.org/10.3390/en5093295.
[16] W.J. Hall, P.T. Williams, Separation and recovery of materials from scrap printed circuit boards, Resour. Conserv. Recycl. 51 (2007) 691–709, https://doi.org/10.1016/j.resconrec.2006.11.010.
[17] Y.M. Kim, S. Kim, J.Y. Lee, Y.K. Park, Pyrolysis reaction pathways of waste epoxy-printed circuit board, Environ. Eng. Sci. 30 (2013) 706–712, https://doi.org/10.1089/ees.2013.0166.
[18] K. Swami, C.D. Judd, J. Orsini, K.X. Yang, L. Husain, Microwave assisted digestion of atmospheric aerosol samples followed by inductively coupled plasma mass spectrometry determination of trace elements, Fresenius. J. Anal. Chem. 369 (2001) 63–70, https://doi.org/10.1007/s002160000575.
[19] W. Chen, Y. Shu, Y. Li, Y. Chen, J. Wei, Co-pyrolysis of waste printed circuit boards with iron compounds for Br-fixing and material recovery, Environ. Sci. Pollut. Res. 28 (2021) 64642–64651, https://doi.org/10.1007/s11356-021-15506-w.
[20] P. Evangelopoulos, E. Kantarelis, W. Yang, Investigation of the thermal decomposition of printed circuit boards (PCBs) via thermogravimetric analysis (TGA) and analytical pyrolysis (Py–GC/MS), J. Anal. Appl. Pyrolysis. 115 (2015) 337–343, https://doi.org/10.1016/j.jaap.2015.08.012.
[21] M. Haghi, F. Fotovat, S. Yaghmaei, Co-pyrolysis of paper-laminated phenolic printed circuit boads and calcium-based additives in fixed and fluidized bed reactors, J. Anal. Appl. Pyrolysis. (2023).
[22] Y. Chen, Y. Zhang, J. Yang, S. Liang, K. Liu, K. Xiao, H. Deng, J. Hu, B. Xiao, Improving bromine fixation in co-pyrolysis of non-metallic fractions of waste printed circuit boards with Bayer red mud, Sci. Total Environ. 639 (2018) 1553–1559, https://doi.org/10.1016/j.scitotenv.2018.05.269.
[23] K.H. Lin, H.L. Chiang, Liquid oil and residual characteristics of printed circuit board recycle by pyrolysis, J. Hazard. Mater. 271 (2014) 258–265, https://doi.org/10.1016/j.jhazmat.2014.02.031.
[24] Y.K. Park, T.U. Han, J. Jeong, Y.M. Kim, Debrominated high quality oil production by the two-step catalytic pyrolysis of phenolic printed circuit boards (PPCB) using natural clays and HY, J. Hazard. Mater. 367 (2019) 50–58, https://doi.org/10.1016/j.jhazmat.2018.12.040.
[25] C. Ma, T. Kamo, Enhanced debromination by Fe particles during the catalytic pyrolysis of non-metallic fractions of printed circuit boards over ZSM-5 and Ni/

SiO_2-Al2O3 catalyst, J. Anal. Appl. Pyrolysis. 138 (2019) 170–177, https://doi.org/10.1016/j.jaap.2018.12.021.
[26] J. Liu, Q. Jiang, H. Wang, J. Li, W. Zhang, Catalytic effect and mechanism of in-situ metals on pyrolysis of FR4 printed circuit boards: insights from kinetics and products, Chemosphere 280 (2021), 130804, https://doi.org/10.1016/j.chemosphere.2021.130804.
[27] J.V.J. Krishna, S.S. Damir, R. Vinu, Pyrolysis of electronic waste and their mixtures: kinetic and pyrolysate composition studies, J. Environ. Chem. Eng. 9 (2021), 105382, https://doi.org/10.1016/j.jece.2021.105382.
[28] G. Grause, M. Furusawa, A. Okuwaki, T. Yoshioka, Pyrolysis of tetrabromobisphenol-a containing paper laminated printed circuit boards, Chemosphere 71 (2008) 872–878, https://doi.org/10.1016/j.chemosphere.2007.11.033.
[29] H.L. Chiang, C.C. Lo, S.Y. Ma, Characteristics of exhaust gas, liquid products, and residues of printed circuit boards using the pyrolysis process, Environ. Sci. Pollut. Res. 17 (2010) 624–633, https://doi.org/10.1007/s11356-009-0245-y.
[30] M.K. Bahng, C. Mukarakate, D.J. Robichaud, M.R. Nimlos, Current technologies for analysis of biomass thermochemical processing: a review, Anal. Chim. Acta. 651 (2009) 117–138, https://doi.org/10.1016/j.aca.2009.08.016.
[31] M. Hu, Z. Chen, D. Guo, C. Liu, B. Xiao, Z. Hu, S. Liu, Thermogravimetric study on pyrolysis kinetics of Chlorella pyrenoidosa and bloom-forming cyanobacteria, Bioresour. Technol. 177 (2015) 41–50, https://doi.org/10.1016/j.biortech.2014.11.061.
[32] G. Várhegyi, P. Szabó, M.J. Antal, Kinetics of charcoal devolatilization, Energy Fuels 16 (2002) 724–731, https://doi.org/10.1021/ef010227v.
[33] C.N. Arenas, M.V. Navarro, J.D. Martínez, Pyrolysis kinetics of biomass wastes using isoconversional methods and the distributed activation energy model, Bioresour. Technol. 288 (2019), 121485, https://doi.org/10.1016/j.biortech.2019.121485.
[34] S. Wang, G. Dai, H. Yang, Z. Luo, Lignocellulosic biomass pyrolysis mechanism: a state-of-the-art review, Prog. Energy Combust. Sci. 62 (2017) 33–86, https://doi.org/10.1016/j.pecs.2017.05.004.
[35] S.A. Scott, J.S. Dennis, J.F. Davidson, A.N. Hayhurst, An algorithm for determining the kinetics of devolatilisation of complex solid fuels from thermogravimetric experiments, Chem. Eng. Sci. 61 (2006) 2339–2348, https://doi.org/10.1016/j.ces.2005.11.002.
[36] J.V.J. Krishna, P.F. Prashanth, R. Vinu, Distributed activation energy modeling and Py-GC/MS studies on pyrolysis of different printed circuit boards for resource recovery, ACS Omega 7 (2022) 31713–31725, https://doi.org/10.1021/acsomega.2c02003.
[37] M. Ahmaruzzaman, Proximate analyses and predicting HHV of chars obtained from cocracking of petroleum vacuum residue with coal, plastics and biomass, Bioresour. Technol. 99 (2008) 5043–5050, https://doi.org/10.1016/j.biortech.2007.09.021.
[38] D.R. Nhuchhen, P. Abdul Salam, Estimation of higher heating value of biomass from proximate analysis: a new approach, Fuel 99 (2012) 55–63, https://doi.org/10.1016/j.fuel.2012.04.015.
[39] Y. Chen, S. Liang, K. Xiao, J. Hu, H. Hou, B. Liu, H. Deng, J. Yang, A cost-effective strategy for metal recovery from waste printed circuit boards via crushing pretreatment combined with pyrolysis: effects of particle size and pyrolysis temperature, J. Clean. Prod. (2021) 280, https://doi.org/10.1016/j.jclepro.2020.124505.
[40] S. Vyazovkin, A.K. Burnham, J.M. Criado, L.A. Pérez-Maqueda, C. Popescu, N. Sbirrazzuoli, ICTAC Kinetics committee recommendations for performing kinetic computations on thermal analysis data, Thermochim. Acta 520 (2011) 1–19, https://doi.org/10.1016/j.tca.2011.03.034.
[41] S. Vyazovkin, Model-free kinetics, J. Therm. Anal. Calorim. 83 (2006) 45–51, https://doi.org/10.1007/s10973-005-7044-6.
[42] Y. Liang, B. Cheng, Y. Si, D. Cao, H. Jiang, G. Han, X. Liu, Thermal decomposition kinetics and characteristics of Spartina alterniflora via thermogravimetric analysis, Renew. Energy. 68 (2014) 111–117, https://doi.org/10.1016/j.renene.2014.01.041.
[43] N. Sbirrazzuoli, Y. Girault, L. Elégant, Simulations for evaluation of kinetic methods in differential scanning calorimetry. Part 1. Application to single-peak methods: freeman-Carroll, Ellerstein, Achar-Brindley-Sharp and multiple linear regression methods, Thermochim. Acta 260 (1995) 147–164, https://doi.org/10.1016/0040-6031(95)90490-5.
[44] H.L. Friedman, Kinetics of thermal degradation of char-forming plastics from thermogravimetry. application to a phenolic plastic, J. Polym. Sci. Part C Polym. Symp. 6 (1964) 183–195, https://doi.org/10.1002/polc.5070060121.
[45] I. Ali, H. Bahaitham, R. Naibulharam, A comprehensive kinetics study of coconut shell waste pyrolysis, Bioresour. Technol. 235 (2017) 1–11, https://doi.org/10.1016/j.biortech.2017.03.089.
[46] J.H. Flynn, L.A. Wall, A quick, direct method for the determination of activation energy from thermogravimetric data, J. Polym. Sci. Part B Polym. Lett. 4 (1966) 323–328, https://doi.org/10.1002/pol.1966.110040504.
[47] T. Akahira, T. Sunose, Method of determining activation deterioration constant of electrical insulating materials, Res. Rep. Chiba. Inst. Technol. Sci. Technol. 16 (1971) 22–31. https://scholar.google.com/scholar_lookup. ?title=Method of determining activation deterioration constant of electrical insulating materials&author=T. Akahira&publication_year=1971&pages=22-31.
[48] A.K. Burnham, R.L. Braun, Global kinetic analysis of complex materials, Energy Fuels 13 (1999) 1–22, https://doi.org/10.1021/ef9800765.
[49] Y. Lin, Z. Chen, M. Dai, S. Fang, Y. Liao, Z. Yu, X. Ma, Co-pyrolysis kinetics of sewage sludge and bagasse using multiple normal distributed activation energy model (M-DAEM), Bioresour. Technol. 259 (2018) 173–180, https://doi.org/10.1016/j.biortech.2018.03.036.
[50] J. Cai, W. Wu, R. Liu, An overview of distributed activation energy model and its application in the pyrolysis of lignocellulosic biomass, Renew. Sustain. Energy Rev. 36 (2014) 236–246, https://doi.org/10.1016/j.rser.2014.04.052.
[51] G. Várhegyi, B. Bobály, E. Jakab, H. Chen, Thermogravimetric study of biomass pyrolysis kinetics. a distributed activation energy model with prediction tests, Energy Fuels 25 (2011) 24–32, https://doi.org/10.1021/ef101079r.
[52] Shi, Y. (2001, May). Particle swarm optimization: developments, applications and resources. In *Proceedings of the 2001 congress on evolutionary computation (IEEE Cat. No. 01TH8546)* (Vol. 1, pp. 81-86). IEEE.
[53] E.D. Dolan, R.M. Lewis, V. Torczon, On the Local Convergence of Pattern Search, SIAM J. Optim. 14 (2003) 567–583, https://doi.org/10.1137/S1052623400374495.
[54] C. Yu, S. Ren, G. Wang, J. Xu, H. Teng, T. Li, C. Huang, C. Wang, Kinetic analysis and modeling of maize straw hydrochar combustion using a multi-Gaussian-distributed activation energy model, Int. J. Miner. Metall. Mater. 29 (2022) 464–472, https://doi.org/10.1007/s12613-021-2305-3.
[55] Q. Xiong, J. Zhang, F. Xu, G. Wiggins, C.Stuart Daw, Coupling DAEM and CFD for simulating biomass fast pyrolysis in fluidized beds, J. Anal. Appl. Pyrolysis. 117 (2016) 176–181, https://doi.org/10.1016/j.jaap.2015.11.015.
[56] A.A. Rostami, M.R. Hajaligol, S.E. Wrenn, A biomass pyrolysis sub-model for CFD applications, Fuel 83 (2004) 1519–1525, https://doi.org/10.1016/j.fuel.2003.09.024.
[57] Y.M. Kim, T.U. Han, C. Watanabe, N. Teramae, Y.K. Park, S. Kim, B. Hwang, Analytical pyrolysis of waste paper laminated phenolic-printed circuit board (PLP-PCB), J. Anal. Appl. Pyrolysis. 115 (2015) 87–95, https://doi.org/10.1016/j.jaap.2015.06.013.
[58] A. Ounas, A. Aboulkas, K. El harfi, A. Bacaoui, A. Yaacoubi, Pyrolysis of olive residue and sugar cane bagasse: non-isothermal thermogravimetric kinetic analysis, Bioresour. Technol. 102 (2011) 11234–11238, https://doi.org/10.1016/j.biortech.2011.09.010.
[59] G. Bhardwaj, M. Kumar, P.K. Mishra, S.N. Upadhyay, Kinetic analysis of the slow pyrolysis of paper wastes, Biomass Convers. Biorefinery. (2021), https://doi.org/10.1007/s13399-021-01363-7.
[60] Y. Chen, J. Yang, Y. Zhang, K. Liu, S. Liang, X. Xu, J. Hu, H. Yao, B. Xiao, Kinetic simulation and prediction of pyrolysis process for non-metallic fraction of waste printed circuit boards by discrete distributed activation energy model compared with isoconversional method, Environ. Sci. Pollut. Res. 25 (2018) 3636–3646, https://doi.org/10.1007/s11356-017-0763-y.
[61] Z. Yao, J. Xiong, S. Yu, W. Su, W. Wu, J. Tang, D. Wu, Kinetic study on the slow pyrolysis of nonmetal fraction of waste printed circuit boards (NMF-WPCBs), Waste Manag. Res. 38 (2020) 903–910, https://doi.org/10.1177/0734242X19896630.
[62] A. Anca-Couce, A. Berger, N. Zobel, How to determine consistent biomass pyrolysis kinetics in a parallel reaction scheme, Fuel 123 (2014) 230–240, https://doi.org/10.1016/j.fuel.2014.01.014.
[63] D. Viju, R. Gautam, R. Vinu, Application of the distributed activation energy model to the kinetic study of pyrolysis of Nannochloropsis oculata, Algal Res. 35 (2018) 168–177, https://doi.org/10.1016/j.algal.2018.08.026.
[64] Z. Yao, S. Yu, W. Su, W. Wu, J. Tang, W. Qi, Kinetic studies on the pyrolysis of plastic waste using a combination of model-fitting and model-free methods, Waste Manag. Res. 38 (2020) 77–85, https://doi.org/10.1177/0734242X19897814.
[65] M... Starink, The determination of activation energy from linear heating rate experiments: a comparison of the accuracy of isoconversion methods, Thermochim. Acta 404 (2003) 163–176, https://doi.org/10.1016/S0040-6031(03)00144-8.
[66] C. Gai, Y. Dong, T. Zhang, The kinetic analysis of the pyrolysis of agricultural residue under non-isothermal conditions, Bioresour. Technol. 127 (2013) 298–305, https://doi.org/10.1016/j.biortech.2012.09.089.
[67] M. Azam, A. Ashraf, S.S. Jahromy, W. Raza, H. Khalid, N. Raza, F. Winter, Isoconversional nonisothermal kinetic analysis of municipal solid waste, refuse-derived fuel, and coal, Energy Sci. Eng. 8 (2020) 3728–3739, https://doi.org/10.1002/ese3.778.
[68] M. Radojević, B. Janković, V. Jovanović, D. Stojiljković, N. Manić, Comparative pyrolysis kinetics of various biomasses based on model-free and DAEM approaches improved with numerical optimization procedure, PLoS One 13 (2018) 1–25, https://doi.org/10.1371/journal.pone.0206657.
[69] J. Xiao, Y. Hu, L. Yang, Y. Cai, L. Song, Z. Chen, W. Fan, Fire retardant synergism between melamine and triphenyl phosphate in poly(butylene terephthalate), Polym. Degrad. Stab. 91 (2006) 2093–2100, https://doi.org/10.1016/j.polymdegradstab.2006.01.018.
[70] Y.C. Lin, J. Cho, G.A. Tompsett, P.R. Westmoreland, G.W. Huber, Kinetics and mechanism of cellulose pyrolysis, J. Phys. Chem. C. 113 (2009) 20097–20107, https://doi.org/10.1021/jp906702p.
[71] J.E. White, W.J. Catallo, B.L. Legendre, Biomass pyrolysis kinetics: a comparative critical review with relevant agricultural residue case studies, J. Anal. Appl. Pyrolysis. 91 (2011) 1–33, https://doi.org/10.1016/j.jaap.2011.01.004.
[72] M. Sobera, J. Hetper, Pyrolysis-gas chromatography-mass spectrometry of cured phenolic resins, J. Chromatogr. A 993 (2003) 131–135, https://doi.org/10.1016/S0021-9673(03)00388-1.
[73] Z. Chen, Y. Chen, H. Liu, Pyrolysis of phenolic resin by TG-MS and FTIR analysis, Adv. Mater. Res. 631–632 (2013) 104–109, https://doi.org/10.4028/www.scientific.net/AMR.631-632.104.
[74] K.A. Trick, T.E. Saliba, Mechanisms of the pyrolysis of phenolic resin in a carbon/phenolic composite, Carbon 33 (1995) 1509–1515, https://doi.org/10.1016/0008-6223(95)00092-R. N. Y.

[75] H. Jiang, J. Wang, S. Wu, B. Wang, Z. Wang, Pyrolysis kinetics of phenol-formaldehyde resin by non-isothermal thermogravimetry, Carbon 48 (2010) 352–358, https://doi.org/10.1016/j.carbon.2009.09.036. N. Y.
[76] G.W. Huber, S. Iborra, A. Corma, Synthesis of transportation fuels from biomass: chemistry, catalysts, and engineering, Chem. Rev. 106 (2006) 4044–4098, https://doi.org/10.1021/cr068360d.
[77] M. Moradi, F. Hasanvandian, A. Bahadoran, A. Shokri, S. Zerangnasrabad, B. Kakavandi, New high-entropy transition-metal sulfide nanoparticles for electrochemical oxygen evolution reaction, Electrochim. Acta. 436 (2022), 141444, https://doi.org/10.1016/j.electacta.2022.141444.
[78] M. Zabeti, T.S. Nguyen, L. Lefferts, H.J. Heeres, K. Seshan, In situ catalytic pyrolysis of lignocellulose using alkali-modified amorphous silica alumina, Bioresour. Technol. 118 (2012) 374–381, https://doi.org/10.1016/j.biortech.2012.05.034.